Good practice guide on high-accuracy GNSS-based distance metrology

EURAMET Technical Guide No. 6
Version 1.0 (02/2025)

Length

Authorship and Imprint

This document was developed by the EURAMET e.V., Technical Committee for Length.
Authors: Sergio Baselga (UPV, Spain), Luis García-Asenjo (UPV, Spain), Pascual Garrigues (UPV, Spain), Raquel Luján (UPV, Spain), Florian Pollinger (PTB, Germany), Ulla Kallio (NLS, Finland), Hannu Koivula (NLS, Finland), Kinga Wezka (WUT, Poland), Dominik Próchniewicz (WUT, Poland), Damien Pesce (IGN, France) and Sten Bergstrand (RISE, Sweden)

The guide was developed within the EMPIR Project 'GeoMetre' (18SIB01) and in cooperation with members of the EURAMET Technical Committee for Length (TC-L). The EMPIR initiative is co-funded by the European Union's Horizon 2020 research and innovation programme and the EMPIR participating states. Funder ID: 10.13039/100014132.

Version 1.0 (02/2025)

EURAMET e.V.
Bundesallee 100
38116 Braunschweig Germany

E-mail: secretariat@euramet.org
Phone: +49 531 592 1960

Official language

The English language version of this document is the definitive version. The EURAMET Secretariat can give permission to translate this text into other languages, subject to certain conditions available on application. In case of any inconsistency between the terms of the translation and the terms of this document, this document shall prevail.

Copyright

ISBN 978-3-942992-90-9

Image on cover page by Raquel Luján.

Guidance publications

This technical guide was developed to provide information on the use of Global Navigation Satellite System (GNSS) techniques for accurate distance determination with assessment of the corresponding uncertainty. Indications on field measurement practices, computation procedures, as well as available products to be used, are given. They differ, in part, from the traditional geodetic approaches where GNSS is used to obtain relative or absolute coordinates instead of the geometric distance, which is the current focus. The estimation of uncertainties in the contributing error sources and their propagation to the distance determined contribute to the traceability and accuracy requirements needed in metrology.

The guide may be used by third parties, e.g. National Accreditation Bodies, peer reviewers, witnesses to measurements, etc., as a reference only. Should the guide be adopted as part of a requirement of any such party, this shall be for that application only and the EURAMET Secretariat should be informed of any such adoption.

On request EURAMET may involve third parties in stakeholder consultations when a review of the guide is planned. If you are interested, please contact the EURAMET Secretariat.

No representation is made nor warranty given that this document or the information contained in it will be suitable for any particular purpose. In no event shall EURAMET, the authors or anyone else involved in the creation of the document be liable for any damages whatsoever arising out of the use of the information contained herein. The parties using the guide shall indemnify EURAMET accordingly.

Further information

For further information about this document, please contact your national contact person of the EURAMET Technical Committee for Length (see www.euramet.org).

Conditions for the Use and Translation of EURAMET Publications

To stimulate international harmonisation of technical procedures in metrology, EURAMET e.V. welcomes the use of its Calibration Guides and Technical Guides by other organisations, e.g. National Metrology Institutes, Regional Metrology Organisations, National Accreditation Bodies, or Regional Accreditation Organisations beyond Europe.

General Information

EURAMET e.V. holds the copyright on all documents developed within its committees.
EURAMET documents may be translated and / or published by other organisations with the permission of EURAMET under the following conditions:

1) the use of the documents is for non-commercial purposes only,
2) resulting documents, in electronic or printed form, shall be distributed free of charge,
3) addenda, e.g. foreword or annexes, may be added, but must be clearly recognisable as such,
4) if a printed version is prepared, four copies shall be sent to the EURAMET Secretariat.

For national dissemination, EURAMET Members or Associates may add the name and/or logo of the National Metrology Institute (NMI) or Designated Institute (DI) to the document. The EURAMET Secretariat must be informed in advance.

Permission to translate or distribute reformatted EURAMET documents, including Calibration Guides and Technical Guides must be obtained from the EURAMET Secretariat in written form by e-mail to: secretariat@euramet.org.

Publication of Calibration Guides and Technical Guides by other Organisations

If an organisation intends to publish a Guide in its own version,

1) the document shall not be modified, except for references to specific European standards, organisations or situations. In this case, modifications must be recognisable as such, e.g. in a footnote,
2) the document may have the organisation's own cover page and registration number. A reference to the original document must be made directly under the registration number as follows: 'This document is identical to [title of the document, version number, publication year]. The copyright of the original version is held by © EURAMET e.V.'

Additionally, the following rules apply if a document is translated into another language.

Translation of EURAMET Publications

If an organisation intends to translate a EURAMET publication,

1) the document shall not be modified and shall be clearly recognisable as a translation of the corresponding EURAMET document,
2) reference must be made to the original document as follows: 'This document is a translation of [title of the document, version number, publication year]. The copyright of the original version is held by © EURAMET e.V.'.

In case of any inconsistency between the terms of the translation and the terms of the original document the original document shall prevail.

EURAMET Technical Guide No. 6

Version 1.0 (02/2025)

Good practice guide on high-accuracy GNSS-based distance metrology

Purpose

This document has been produced to suggest good practices on the use of Global Navigation Satellite System (GNSS) techniques for accurate distance determination.

Content

1 INTRODUCTION

The purpose of this document is to suggest good practices on the use of global navigation satellite system (GNSS) techniques for accurate distance determination in the open field over distances of up to several kilometres with uncertainties of a few millimetres or better. Guidelines are given for field measurements, computation procedures, as well as available products to be used. They are different from the traditional geodetic approaches where GNSS is used to obtain relative or absolute coordinates instead of the geometric distance, which is the current focus, and conform what we name a GNSS-based distance meter (GBDM). The guideline is based on the knowledge produced under the EMPIR Project 'GeoMetre' (18SIB01) [1], the previous good practice guide published by the EMRP JRP Surveying (SIB60) Consortium [2], and the published papers cited in the document, in particular [3] and [4]. In the first part (sections 2, 3 and 4), the scope, equipment and functional model are given. The second part of this guideline, sections 5 and 6, give the estimation of uncertainties and the propagation to the final distance. Section 7 gives application examples of these procedures.

2 SCOPE AND FIELD OF APPLICATION

This guideline refers to the accurate determination of lengths up to several kilometres in the field with uncertainties of a few millimetres or better by means of GNSS. The methodology for a GNSS-based distance meter (GBDM) is different from the traditional geodetic methods used in GNSS processing aimed at obtaining three-dimensional coordinates, be they absolute (station coordinates) or relative to a point (baseline components) since the distance and its corresponding uncertainty are the only parameters to be determined and the selected observables and methods can be chosen accordingly.

The determination of distances in the open field with uncertainties of 1 mm or better is being increasingly required for different applications, including the determination of local ties in Fundamental Geodetic Observatories [5], construction of large-scale facilities such as particle accelerators [6], calibration baselines [7], deformation monitoring of critical infrastructures [8], and monitoring of geological hazards such as volcanoes or faults [9]. The use of high precision Electronic Distance Meters (EDMs) is limited by the required accurate determination of the index of refraction along the light path, which is a difficult task, and the need for a clear line of sight.

The metre, SI unit of length, is defined by taking the value of the speed of light in vacuum, c, to be 299 792 458 m s^{-1} [10]. Therefore, two main types of error contributions have to be considered in the GNSS traceability chain: time measurement and the propagation in a material medium other than vacuum.

Regarding time measurement, GNSS measurements can be traced to the definition of the second (in the satellite end) by means of the use of atomic clocks both by the satellites and by the constellation ground control network, as explained in [11]. As regards the definition of time in the receiver end, it is one unknown of the system of observation equations that cancels after the double differencing strategy except for the case of very large time offsets: this is the reason why the offsets of receiver clocks are estimated along with their uncertainties in the Precise Point Positioning (PPP) estimation, as mentioned in the guide.

Regarding the propagation in a medium other than vacuum, the consideration of the signal delays in the propagation through the atmosphere have to be taken into account along with their corresponding uncertainty: these are the ionospheric and tropospheric delays, which are discussed in the guide, along with other perturbative effects taking place in practice: the multipath effect and (the calibration of) the antenna reception point and the antenna height.

The use of a GBDM is appealing for several reasons: first, the worldwide GNSS scale stability at the level of 0.001 ppm (or 1 ppb) [5,12]; second, GNSS instrumentation is readily available in metrology centers, research institutes and private companies and a methodology based on its use can be easily adopted; and third, certain observing conditions (for example, lack of direct intervisibility between the baseline ends) may be a problem for the use of other techniques. The JRP SIB60 Metrology for long distance surveying project summarized their research on this topic, though limited to distances up to 1 km, in their *Good practice guide for high accuracy global navigation satellite system based distance metrology* [2]. As it was concluded, the “propagation of the signal through the ionosphere and troposphere, effect of multipath, antenna phase center variations and other sources of error are not controllable and are mostly unknown during the data processing. Although one can estimate the magnitude of these variables in the analysis, uncertainties of these estimations are mostly unknown, and especially their propagation into the final results”. It was also remarked that the user has little information on the propagation of uncertainties when using standard software packages. As concluded in [2], this all prevents a stringent uncertainty analysis of a distance measurement performed by GNSS. In the present guide, we want to make a step forward in the application of GNSS to open air length metrology and remedy as much as possible these detected limitations. The present guide is based in the knowledge gained under the EMPIR Project 'GeoMetre' (18SIB01), which has been mainly presented in [4]. We define a relatively simple strategy for use in length metrology that makes use of renowned standards for GNSS files and products (RINEX for GNSS data files, SP3 as provided by International GNSS Service (IGS) for final ephemerides of satellites, ANTEX files as provided by IGS for satellite antenna phase center offsets and variations and ANTEX files for individual antenna calibrations at the user end), an initial PPP to characterize error sources at the zero differences level, and a processing strategy specially tailored to the optimal determination of the distance and its corresponding uncertainty as rigorously propagated through the equations by which the distance is finally determined from the uncertainties of the error sources estimated in zero differences.

Thus, this guide provides a measurement and analysis strategy to derive distances by GBDM together with a GUM-conformal estimation of a measurement uncertainty. We assume the reader to be familiar with the main concepts of GNSS instrumentation (receivers, antennas and auxiliary equipment), and geodetic processing, be it in absolute mode, PPP in particular, or in relative mode, specifically by means of double-difference carrier phase equations.

3 EQUIPMENT AND DATA

The minimum equipment for the determination of a baseline length at the targeted uncertainty level consists of two high-grade multi-frequency receivers and two individually calibrated high-grade geodetic antennas (of choke ring type and preferably of the same model), each with the necessary auxiliary equipment (battery, memory, tribrach, handheld compass). In what follows it is assumed that the benchmarks defining the baseline whose distance is to be determined are geodetic pillars. As in the Good practice guide [2], the use of identical antenna types and mountings at both ends of the distance is strongly recommended to create the same near field.

Since the usual determination of antenna heights with folding rules is insufficient and not recommended [2], additional equipment and methodology may be required for accurately determining each antenna height above the top of the pillar. A general method based on a precise total station along with its reflector is described in Section 5.5.

For the station set-up the antennas shall be oriented towards the North, the auxiliary material (tribrach, centering adaptor, etc.) shall be identical in both baseline ends, and the antenna cable routing shall be the same and fixed avoiding loose cable parts. Additionally, meteorological stations may be required if a model for the lower troposphere is externally estimated to correct the differential tropospheric delay from field measurements.

Regarding the observation duration, at least 24 hours are recommended so that the residual periodic effects can be averaged out, or, preferably several days, three or four, as in [13]. Also in agreement with [2], the use of L1 carrier phase observations is preferred as long as the influence of the ionosphere in the double-differenced equations can be neglected or eliminated with sufficient accuracy (see Section 5.2).

The following data and following standard file types are then assumed to be available:

- GNSS observation files, in RINEX format.
- Precise satellite ephemerides and clocks files, in SP3 format as provided by the IGS.
- Satellite antenna phase center offsets and variations, ANTEX file as provided by the IGS.
- Individual antenna calibrations (at least by one method) for each of the available antennas, in ANTEX format.

It is well-known that most of the errors affecting the GNSS positioning are largely cancelled by forming double differences (two satellites, two receivers); the GBDM strategy is therefore based on double-differenced carrier phases. Understanding, however, that the error sources occur at the zero differences level, that is in the satellite-to-receiver direction, these errors need to be, first, rigorously estimated at this level (size, sign and uncertainty of the corresponding estimation), so that the observables can be appropriately corrected, and then the corresponding uncertainty in the correction be propagated to the final result through the particular double-differences equations by which the distance is determined in each case. Therefore, a PPP processing is initially carried out with the observed data and part of its by-products are subsequently used in the double-difference processing [14].

Although one could obtain this initial information from the use of scientific packages like Bernese [15], commercial solutions or user-developed software, the use of the online free CSRS-PPP service (version 3) [16] is here suggested and exemplarily discussed as a simple, easy-to-use means to obtain a set of initial information that is both internally consistent as well as consistent with standard up-to-date IGS products. The CSRS-PPP service provides a PPP processing with Ambiguity Resolution (PPP-AR), a proven strategy to obtain reliable results. Secondly, it allows the user to upload to its website observation RINEX files not limited to 24 h (as in other services), and thirdly, the detailed information on the processing and results are almost immediately emailed to the user: station coordinates referred to the mean observation epoch with high quality (typical uncertainties of a few mm for 24 h observation files), excellent tropospheric estimates [17,18] along with their corresponding uncertainties, receiver clocks, observation carrier phase residuals, detailed plots, etc.

The necessary results of this initial processing are Earth-Centered Earth-Fixed (ECEF) approximate coordinates for both stations, estimated clock offsets for both stations (to avoid the harmful effect of receiver clocks with very large offsets, not completely cancelled in practice after double differencing), tropospheric delays, and carrier phase residuals.

4 FUNCTIONAL MODEL

A model based on double-differenced carrier phase equations, where the relevant error sources have been corrected at the zero-differenced level with the use of auxiliary information is the base for the current approach. The effects corrected at the zero-differenced level include: satellite and receiver clocks (corrected with IGS satellite clocks and CSRS-PPP computed clocks), satellite and receiver antenna calibration values (IGS ANTEX files for satellite antennas and ANTEX files for individually calibrated receiver antennas), tropospheric delays (from CSRS-PPP computed values), multipath effects (from a multipath model obtained by sidereal filtering of consecutive days).

The double-differenced carrier phase equation for a pair of receivers *i* and *j* and a pair of satellites *k* and *l* can be written [4] as

$$\lambda\varphi_{ij}^{kl} - \rho_{ij0}^{kl} - \lambda N_{ij}^{kl} + I_{ij}^{kl} - T_{ij}^{kl} - MP_{ij}^{kl} - \varepsilon_{ij}^{kl} = \left(\frac{\partial\rho_{ij}^{kl}}{\partial X_j}\right)_0 dX_j + \left(\frac{\partial\rho_{ij}^{kl}}{\partial Y_j}\right)_0 dY_j + \left(\frac{\partial\rho_{ij}^{kl}}{\partial Z_j}\right)_0 dZ_j \quad (1)$$

where the approximate coordinates of the endpoint *i* are being held fixed and the displacement in coordinates are being attributed to changes in coordinates of station *j* only (dX_j, dY_j, dZ_j), a simplification which has a completely negligible impact for baselines up the current lengths (a few kilometres at the most). The terms appearing in Eq. (1) are defined next

λ	carrier phase wavelength in vacuum, in m
φ_{ij}^{kl}	double-differenced carrier phase, in cycles
ρ_{ij0}^{kl}	double-differenced geometric distance between satellites and receivers, using approximate coordinates for *i* and *j*, in m

N_{ij}^{kl}	double-differenced ambiguity
I_{ij}^{kl}	double-differenced ionospheric delay, in m
T_{ij}^{kl}	double-differenced tropospheric delay, in m
MP_{ij}^{kl}	double-differenced multipath, in m
ε_{ij}^{kl}	double-differenced observation error, in m
$\left(\frac{\partial \rho_{ij}^{kl}}{\partial X_j}\right)_0$	partial derivative of the double-differences geometric distance with respect to coordinate X_j particularised for the approximate coordinates of *i* and *j*
dX_j	correction to approximate coordinates X_j, in m
$\left(\frac{\partial \rho_{ij}^{kl}}{\partial Y_j}\right)_0$	partial derivative of the double-differences geometric distance with respect to coordinate Y_j particularised for the approximate coordinates of *i* and *j*
dY_j	correction to approximate coordinates Y_j, in m
$\left(\frac{\partial \rho_{ij}^{kl}}{\partial Z_j}\right)_0$	partial derivative of the double-differences geometric distance with respect to coordinate Z_j particularised for the approximate coordinates of *i* and *j*
dZ_j	correction to approximate coordinates Z_j, in m

The correction values from the individual antenna calibrations are assumed to have been already included in the computed double-differenced carrier phase. Possible cycle slips are assumed to have been repaired before the adjustment. Other sources of error of the GNSS systems not explicitly included above are not relevant to our double differences approach. They completely cancel out: this is the case, for example, of relativistic effects, which cancel for all practical purposes in relative positioning ([19] p.229), and the windup effect, which is “completely cancelled in double differences” [20, p.731].

All the terms in the left-hand side of Eq. (1), except ε_{ij}^{kl}, are then known or can be determined as explained in the next section, so that for the entire set of observations a system of double-differenced equations

$$\boldsymbol{k} + \boldsymbol{r} = \boldsymbol{A}\boldsymbol{x} \tag{2}$$

can be formed, where $\boldsymbol{k}$ is the vector of independent terms (observed minus computed double differences), $\boldsymbol{r}$ is the residual vector (with elements of the type $-\varepsilon_{ij}^{kl}$, and $\boldsymbol{x}$ is the vector of unknowns

$$\boldsymbol{x} = \begin{pmatrix} dX_j \\ dY_j \\ dZ_j \end{pmatrix} \tag{3}$$

Using the relationship between the distance *D*, azimuth α and local height difference *z* and the increments of local geodetic coordinates *x*, *y* and *z* (easting, northing, upping),

first, and then the relationship between these increments and the increments of coordinates *X*, *Y* and *Z* in the ECEF system, second, the vector of unknowns can be written as

$$\begin{pmatrix} dX_{ij} \\ dY_{ij} \\ dZ_{ij} \end{pmatrix} = \boldsymbol{RJ}^{-1} \begin{pmatrix} dD_{ij} \\ d\alpha_{ij} \\ dz_{ij} \end{pmatrix} \tag{4}$$

using the corresponding rotation and Jacobian matrices ***R*** and ***J*** (see more details in [4]), and in the case where the displacement is only attributed to *j*, as

$$\begin{pmatrix} dX_{j} \\ dY_{j} \\ dZ_{j} \end{pmatrix} = \boldsymbol{RJ}^{-1} \begin{pmatrix} dD_{ij} \\ d\alpha_{ij} \\ dz_{ij} \end{pmatrix} \tag{5}$$

Including Eqs. (3) and (5) in the right-hand side of Eq. (2) it can be written

$$\boldsymbol{k} + \boldsymbol{r} = \boldsymbol{ARJ}^{-1} \begin{pmatrix} dD_{ij} \\ d\alpha_{ij} \\ dz_{ij} \end{pmatrix} \tag{6}$$

and

$$\boldsymbol{k} + \boldsymbol{r} = \boldsymbol{B} \begin{pmatrix} dD_{ij} \\ d\alpha_{ij} \\ dz_{ij} \end{pmatrix} \tag{7}$$

defining a new matrix ***B***

$$\boldsymbol{B} = \boldsymbol{ARJ}^{-1} \tag{8}$$

The new unknown vector in Eq. (7)

$$\boldsymbol{x}' = \begin{pmatrix} dD_{ij} \\ d\alpha_{ij} \\ dz_{ij} \end{pmatrix} \tag{9}$$

can be determined by a least-squares adjustment as

$$\boldsymbol{x}' = \left(\boldsymbol{B}^{\boldsymbol{T}}\boldsymbol{PB}\right)^{-1}\boldsymbol{B}^{\boldsymbol{T}}\boldsymbol{Pk} \tag{10}$$

where ***P*** is the weight matrix of the equation system, so that the first unknown ***x'***(1) yields

the correction to the initial approximate distance in terms of the approximate coordinates used for the receivers, dD_{ij}, and its corresponding precision can be found in the first element of the covariance matrix, $\boldsymbol{C}_{\boldsymbol{x}'}(1,1)$, which is obtained as

$$\boldsymbol{C}_{\boldsymbol{x}'} = \hat{\sigma}_0{}^2 \left(\boldsymbol{B}^{\boldsymbol{T}} \boldsymbol{P} \boldsymbol{B}\right)^{-1} \tag{11}$$

where

$$\hat{\sigma}_0{}^2 = \frac{(\boldsymbol{r}^{\boldsymbol{T}} \boldsymbol{P} \boldsymbol{r})}{m-n} \tag{12}$$

is the variance of unit weight, for the number of observations m and the number of unknowns $n = 3$.

5 ERROR AND UNCERTAINTY ESTIMATION

We show now how the errors in the left-hand side of Eq. (1) can be corrected and their corresponding uncertainties estimated. The analysis is initially done for a particular time instant at the zero differences level, that is, referred to the satellite-to-receiver direction observation. The estimates will be then propagated to the double-differences equations, first, and then to the final distance obtained after the least squares adjustment.

Since the errors in the observed carrier phases are included in the residual term and subsequently estimated in the adjustment, and the impact of the errors due to the inaccuracies of the approximate coordinates can be neglected (as shown in [21] they do not cause a significant impact provided their accuracies are of 1-2 cm or better, as is the current case after the PPP processing), the first term to determine is the ambiguity term.

In the case of horizontal baselines below one kilometre and low multipath, ambiguities can be easily determined by rounding them to the nearest integer [3]. This is not applicable, however, to the case of baselines up to several kilometres with a possibly significant height difference, where, no matter how close to their exact values the approximate coordinates are, the rounding to the nearest integer strategy does not always work because of the effect of the remaining corrections (ionospheric and tropospheric delays, and multipath effect). Ambiguity determination is then needed. One possibility is to use the values obtained after the PPP: in the case of the CSRS-PPP the integer nature of the ambiguities is considered in the functional model, as in Eq. (1). Alternatively, two different easy procedures prove to have a high ambiguity success rate:

- solving the system of equations to obtain floating ambiguities and then rounding them to their nearest integers.
- setting to zero the coordinate corrections $dX_j = 0$, $dY_j = 0$, and $dZ_j = 0$ in Eq. (1), which is sensible due to the accurate initial PPP processing, and obtaining ambiguities by solving the simplified system of equations: first as floating ambiguities and then rounded to their nearest integer.

By using both determinations above an even higher degree of security is obtained for the coincident ambiguities. We are now concerned with the estimation of the different corrections involved in Eq. (1) and their corresponding uncertainties.

5.1 Tropospheric delay

For baselines up to several kilometres with possibly significant height differences (even hundreds of meters) tropospheric delays do not necessarily cancel out in the double differences. As a possible standard (or initial) method, we therefore recommend using the values of tropospheric delay estimated by the CSRS-PPP service to compute the double differenced corrections to be subtracted in the left-hand side of Eq. (1), and using the corresponding uncertainties also provided by the CSRS-PPP to obtain the uncertainties in the double differences, first, and then in the final estimation of the baseline distance. Alternatively, tropospheric delay estimates obtained by PPP with Bernese or other software can be used.

The uncertainties in the tropospheric delay corrections are given by the CSRS-PPP service for the zenith directions, that is u_{T_j} and u_{T_i} for stations *j* and *i*, respectively. They need to be mapped to the corresponding receiver-to-satellite line of sight by a mapping function. Different mapping functions have been proposed in the literature. Black and Eisner's mapping [22]

$$m_j^l = \frac{1.001}{\sqrt{0.002001 + \sin^2 E_j^l}} \tag{13}$$

is a simple mapping function in terms of the elevation of satellite l seen from receiver j, E_j^l. More elaborate and accurate functions exist, such as the Niell Mapping Function (NMF) [23], Vienna Mapping Function 1 (VMF1) [24], or the Global Mapping Function [25]. The use of NMF, VMF1 and GMF yields differences of the order of millimetres in the computation of the tropospheric delays but provides completely negligible differences when used to compute the double differenced tropospheric delays, while for the purpose of computing the uncertainty propagation it is sufficient to use the formula above, that is, the uncertainty in the zero differenced tropospheric delay can be obtained as

$$u_{T_j^l} = m_j^l u_{T_j} \tag{14}$$

using the mapping function defined in Eq. (13)

5.2 Ionospheric delay

In a similar way to the case of the tropospheric delays, the best approach would be to use ionospheric delay corrections for the observations from each station along with their estimated uncertainties. Since this information is currently not provided by GNSS services like the CSRS-PPP, the best possibility is using a combination of L1 and L2 GPS carrier phases (or E1 and E5a for Galileo) that eliminates the ionospheric delay to the first order, such as the one that is often named as L3 [15]

$$\varphi_3 = 77\varphi_1 - 60\varphi_2 \tag{15}$$

where φ_1, φ_2 and φ_3 are the carrier phases of L1, L2 and L3, respectively, in unit cycles or, equivalently

$$\Phi_3 = \frac{{f_1}^2}{{f_1}^2 - {f_2}^2}\,\Phi_1 - \frac{{f_2}^2}{{f_1}^2 - {f_2}^2}\,\Phi_2 \qquad (16)$$

where Φ_1, Φ_2 and Φ_3 are the carrier phases in m for L1, L2 and L3, respectively, and f_1 and f_2 are the carrier frequencies of L1 and L2.

Although these combinations of L1 and L2 (or E1 and E5a) are indeed quasi ionosphere-free, the existing residual error is eliminated after double differencing (with a negligible uncertainty). Alternatively, a combination of three frequencies can be used. The cost, both for the dual frequency combination and, even more so, for the triple frequency case, is an increase in noise compared to using L1 alone (by a factor of approximately 3 for the case of L3 [15, p.53]).

Another possibility is the use of the Klobuchar model. Although it is estimated that this model cannot correct more than 50 % of the delay at zero differences, the calculation of the double differences largely cancels out the residual error and does not have a significant impact on the final distance. There are other possibilities to correct for ionospheric delays that could be explored as well, such as the use of Real-time TEC mapping provided it has enough resolution to give significantly different correction values for the two baseline endpoints, which are only a few kilometers apart.

5.3 Multipath effect

A careful selection of the observing site, when possible, together with the use of choke ring antennas and long observing times are the best advice to minimize the multipath effect. At the computational level it is difficult to assess the existing multipath effect so that obtaining a reliable estimate of the multipath error affecting each observation (along with an uncertainty for this estimate) is a complicated task.

For the case of GPS observations, however, we suggest using the sidereal filtering technique, provided observations in different days are available, which is based on the apparent repeating period of the GPS constellation of one sidereal day. For other constellations this is not practical due to their longer apparent repeating periods. Due to the short observation campaign (a few consecutive days) it is assumed that there are no big changes of vegetation, water or snow significantly varying the multipath effect during the campaign.

As explained in [3], the sidereal filtering technique assumes that all significant sources of error have been taken into account so that the observation residuals (in our case the residuals obtained after the CSRS-PPP processing) contain mostly multipath. For every observing site and every satellite, the observation residuals of different consecutive sidereal days can be matched so that a time-varying multipath model can be constructed for each satellite and observing site. The residual matching is best done by using the closest satellite azimuth and elevation values between the days or, secondly preferred (because the repeat period deviates slightly from one sidereal day differently for each satellite), by simply shifting the residuals by one, or more, sidereal days. Three or more observing days are advisable to construct this model.

This model (see [3, Fig. 5] or the Application Examples Section of this guide) does not only yield the value of the multipath correction (the average values) but also an estimate of its uncertainty (the experimental dispersion).

Beyond the restriction of the use of this technique to GPS observations, it must be noted that the decimation of the CSRS-PPP observations at 30 s significantly hampers the application of the sidereal filtering technique, since it only allows a relatively poor satellite matching from 30 s observation rates instead of the more accurate definition that could be obtained, for example, using observation rates of 1 s. Alternative computation of the sample of residuals, by a user-developed software for example, might be disadvantageous, however, by breaking the consistency in the set of auxiliary estimates used (that is, coordinates, clocks, observation residuals, tropospheric corrections and ionospheric corrections, all of them derived from CSRS-PPP).

5.4 Antenna calibration

The signal reception point at the antenna is not a fixed point that can be mechanically identified, but varies with the frequency, azimuth and elevation of the incoming signal. Thus, in addition to the Antenna Reference Point (ARP), which is the only point that is externally accessible to the user, a Phase Center Offset (PCO), taken as a mean value for the entire range of satellite azimuth and elevation, and an additional Phase Center Variation (PCV), dependent on the particular azimuth and elevation of the line of sight from receiver to satellite, are required to be known. These are given for each signal frequency in the GNSS antenna calibrations files, which may originate from a general calibration or from an individual calibration of the particular antenna by a dedicated procedure.

ATX IGS antenna calibration files are the standard files of general calibration type. They offer mean calibration values for each type of antenna (PCOs and tabulated PCVs in terms of azimuth and elevation, for each signal frequency) after the calibration of different antennas of the same model. Individual calibration files, on the contrary, are obtained by a dedicated method, such as robot calibration or anechoic chamber, to individually characterize the particular antenna. In real practice, however, when setting up a calibrated antenna on a particular monument, the surrounding electromagnetic field may have an impact in the antenna reception point. This is hard to be modelled but, with the proposed strategy, the error will be mitigated by the use of the sidereal filtering technique because this mismodeled error would have a similar behavior to periodic multipath.

Special methods for quantifying the errors, validating and comparing GNSS antenna calibrations have been recently presented [26,27]. To determine the baseline distance along with its corresponding uncertainty propagated from the original error sources, we need to estimate and incorporate into the uncertainty budget the amount of uncertainty attributed to the antenna calibration in use. Since the present document aims to propose simple methods using, where possible, standard products and solutions, it is proposed to compare the values from the individual robot calibration versus those from the individual anechoic chamber calibration (as they are the leading methods for antenna calibration), provided they are both available for the antenna in use, or, alternatively, to compare any available individual calibration versus the generic calibration, so that the difference between both calibrations is taken as the uncertainty (k = 1) of the individual calibration correction. These uncertainties at the level of zero differences will be then propagated to double differences, and subsequently to the baseline distance.

5.5 Antenna height

If accurate centering systems are used, the uncertainty in the antenna horizontal centering can be neglected. The measurement of the antenna height is especially critical, however. As acknowledged in the good practice guide [2, p.13] the use of a ruler or folding tape is insufficient. This is particularly true for high elevation differences between the baseline endpoints, where it is possible that one third of the uncertainty in the antenna height determination propagates to uncertainty in the baseline distance [4].

A relatively simple field strategy based on the use of a total station (TS) to accurately determine the antenna height and its corresponding uncertainty, similar to the one proposed in [4] is presented here. The uncertainties in the determination of antenna heights in both endpoints will be then propagated to the final distance. As previously said, it is assumed that each benchmark is a geodetic pillar, although the proposed procedure could be easily adapted to other possible cases of interest.

The following steps are described in the recommended order of operation at the beginning of the GNSS observation. They can also be followed, in reverse order, at the end of the GNSS measurement to obtain an additional determination of the antenna height.

First, the TS is set up a few meters apart from the pillar, where a suitable pointing device of known height, h_d, has been installed, Fig. 5.1. The vertical angle to the pointing device, V_d, is accurately measured. In the next step, the reduced – or horizontal – distance, D_R, also depicted here, will be determined eventually allowing for the increment of height Δz_d to be known.

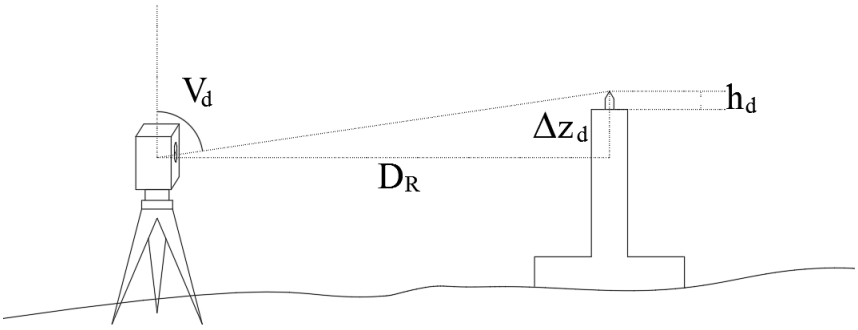

Figure 5.1. Vertical angle measurement to the top of the pointing device

The pointing device is then removed and a tribrach with a prism reflector is installed on the pillar, Fig. 5.2. It is essential that the tribrach is levelled at this point and that the levelness is not changed when the GNSS antenna is also placed on top of it in the next step.

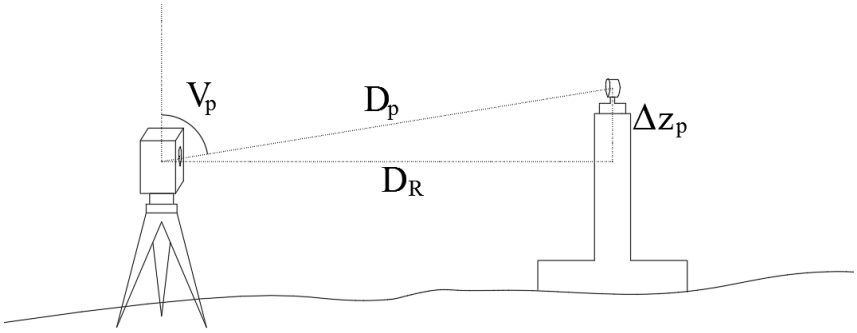

Figure 5.2. Vertical angle and distance measurement to a prism

The measurement of the vertical angle V_p and geometric distance D_p to the prism permits to obtain the reduced distance D_R by means of

$$D_R = D_p \sin V_p \tag{17}$$

as well as the height difference Δz_p by means of

$$\Delta z_p = \frac{D_R}{\tan V_p} \tag{18}$$

Also the height difference to the pointing device, Fig. 5.1, can be obtained now as

$$\Delta z_d = \frac{D_R}{\tan V_d} \tag{19}$$

The antenna is then set up on the levelled tribrach and the vertical angle to a well-defined part of the antenna (here the tangent to its rounded top), V_a, is measured, Fig. 5.3.

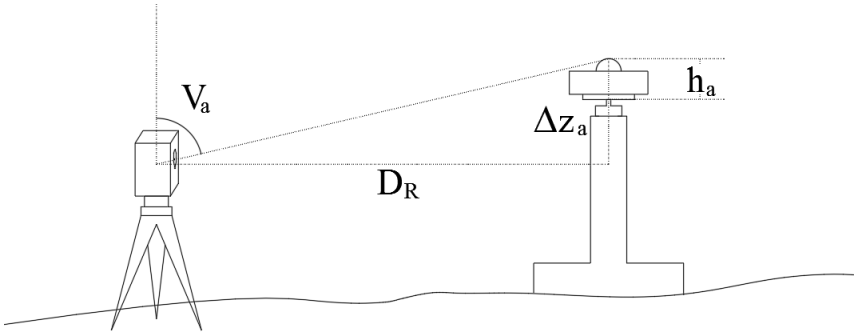

Figure 5.3. Vertical angle measurement to a well-defined part of the antenna

Laboratory measurements or, alternatively, the use of the antenna's design specifications, are needed to provide an accurate value for the offset h_a between the measured point and the base of the antenna (standard antenna height reference).

The height difference Δz_a can now be computed by means of

$$\Delta z_a = \frac{D_R}{\tan V_a} \tag{20}$$

If we subtract h_a from Δz_a we have the height of the base of the antenna over the TS horizontal axis, whereas in Fig. 5.1 we can see that subtracting h_d from Δz_d gives the height of the top of the pillar over the TS horizontal axis. We can therefore obtain the height of the base of the antenna over the top of the pillar, let us denote it by h, as

$$h = (\Delta z_a - h_a) - (\Delta z_d - h_d) \tag{21}$$

or

$$h = D_p \sin V_p \left(\frac{1}{\tan V_a} - \frac{1}{\tan V_d}\right) + h_d - h_a \tag{22}$$

To compute the uncertainty in the antenna height u_h, the law of error propagation must be applied to Eq. (22) in terms of the uncertainties in the measured values D_p, V_p, V_a, V_d, h_d, and h_a, respectively, u_{Dp}, u_{Vp}, u_{Va}, u_{Vd}, u_{hd} and u_{ha}. That is

$$u_h{}^2 = \left(\frac{\partial h}{\partial D_p}\right)^2 u_{D_p}{}^2 + \left(\frac{\partial h}{\partial V_p}\right)^2 u_{V_p}{}^2 + \left(\frac{\partial h}{\partial V_a}\right)^2 u_{V_a}{}^2 + \left(\frac{\partial h}{\partial V_d}\right)^2 u_{V_d}{}^2 + u_{h_d}{}^2 + u_{h_a}{}^2 \tag{23}$$

Usually, the heights h_d and h_a can be known much more accurately than the rest of the measurands and their contribution to the uncertainty in the antenna height is not significant. Then

$$u_h{}^2 = \left(\frac{\partial h}{\partial D_p}\right)^2 u_{D_p}{}^2 + \left(\frac{\partial h}{\partial V_p}\right)^2 u_{V_p}{}^2 + \left(\frac{\partial h}{\partial V_a}\right)^2 u_{V_a}{}^2 + \left(\frac{\partial h}{\partial V_d}\right)^2 u_{V_d}{}^2 \tag{24}$$

with

$$\frac{\partial h}{\partial D_p} = \sin V_p \left(\frac{1}{\tan V_a} - \frac{1}{\tan V_d}\right) \tag{25}$$

$$\frac{\partial h}{\partial V_p} = D_p \cos V_p \left(\frac{1}{\tan V_a} - \frac{1}{\tan V_d}\right) \tag{26}$$

$$\frac{\partial h}{\partial V_a} = -D_p \sin V_p \frac{1}{\sin^2 V_a} \tag{27}$$

$$\frac{\partial h}{\partial V_d} = -D_p \sin V_p \frac{1}{\sin^2 V_d} \tag{28}$$

Assuming the same uncertainty u_V in the determination of all vertical angles and approximating all squared sines of vertical angles to 1 (with no loss of significant accuracy due to their closeness to the square angle) and the squared cosine of a vertical angle to zero (for the same reason) we can obtain

$$u_h{}^2 = \left(\frac{1}{\tan V_a} - \frac{1}{\tan V_d}\right)^2 u_{D_p}{}^2 + 2D_p{}^2 u_V{}^2 \tag{29}$$

5.6 Monument stability

The stability of the monuments during the time that the observation lasts, or in the long term if it is desired to obtain a significant value over time (for example in the case of a geodetic network, which is of permanent use), must be adequately estimated. This instability will contribute to the final distance as explained in the following section.

As shown in [28], masts should be avoided in the cases where the highest accuracy is sought for, since, except for truss masts, masts normally experience daily movements higher than 1 mm [28].

The best choice seems to be the use of reinforced concrete pillars with an isolation air chamber to avoid thermal dilations. The deformation of the pillar by changes in the temperature has been studied in detail and reported in [29], and has been found to occur mainly in the horizontal direction with a maximum displacement that can be modelled as

$$w = k\Delta T \tag{30}$$

with

$$k = \alpha_T \frac{L^2}{2d} \tag{31}$$

$$\alpha_T = 1.241{\times}10^{-5}\ K^{-1} \tag{32}$$

where w is the displacement in mm, ΔT is the change of temperature in K, and L and d are the height and diameter of the pillar, respectively, in mm.

If no other quantification of the pillar movements is available for the case at hand it is suggested to use the values provided by these formulas.

6 UNCERTAINTY PROPAGATION

6.1 Propagation from zero to double differences

Except for the cases of the uncertainty in antenna height determination and monument stability, which will be analyzed at the end of the next subsection, subsection 6.2, the propagation of a particular error source from zero differences, say e_j^l, e_j^k, e_i^l and e_i^k, to double differences, say e_{ij}^{kl} may take two different forms. The first one refers to an error type e that can be computed by a zenith error mapped to the receiver-to-satellite direction by a suitable mapping function. This is the case of the tropospheric and ionospheric delays (though usually with different mapping function types). The second form, where mapping functions and zenith errors are concepts not applicable to the particular error, is the case of the multipath effect and the antenna phase center offset and variations.

In the first case, that is, where there is a zenith error above the station, say e_i and e_j for stations i and j, respectively, and a suitable mapping function for the receiver-to-satellite direction, we can write

$$e_j^l = m_j^l e_j \quad (33)$$
$$e_i^l = m_i^l e_i \quad (34)$$
$$e_j^k = m_j^k e_j \quad (35)$$
$$e_i^k = m_i^k e_i \quad (36)$$

where m_j^l, m_j^k, m_i^l and m_i^k are the mapping function for stations *i* and *j* and satellites *k* and *l*, and e is the error (in tropospheric and ionospheric delay, respectively) to be corrected in the observation equation.

Denoting by $u_{e_j^l}$, $u_{e_j^k}$, $u_{e_i^l}$ and $u_{e_i^k}$ the corresponding uncertainties of the errors e_j^l, e_j^k, e_i^l and e_i^k, which can be obtained as

$$u_{e_j^l} = m_j^l u_{e_j} \quad (37)$$
$$u_{e_i^l} = m_i^l u_{e_i} \quad (38)$$
$$u_{e_j^k} = m_j^k u_{e_j} \quad (39)$$
$$u_{e_i^k} = m_i^k u_{e_i} \quad (40)$$

where u_{e_j} and u_{e_i} are the corresponding uncertainties of the zenith errors e_j and e_i and we have assumed that the mapping functions have a completely negligible error for the purpose of uncertainty propagation.

Applying the law of covariance propagation to Eqs. (33-36) it is obtained

$$u_{e_j^l e_i^l} = m_j^l m_i^l u_{e_{ji}} \quad (41)$$
$$u_{e_j^k e_i^k} = m_j^k m_i^k u_{e_{ji}} \quad (42)$$
$$u_{e_j^l e_i^k} = m_j^l m_i^k u_{e_{ji}} \quad (43)$$
$$u_{e_j^k e_i^l} = m_j^k m_i^l u_{e_{ji}} \quad (44)$$
$$u_{e_j^l e_j^k} = m_j^l m_j^k {u_{e_j}}^2 \quad (45)$$
$$u_{e_i^l e_i^k} = m_i^l m_i^k {u_{e_i}}^2 \quad (46)$$

in terms of the variances and covariance of the zenith errors in *j* and *i*, ${u_{e_j}}^2$, ${u_{e_i}}^2$ and $u_{e_{ji}}$, respectively.

Now for the double difference

$$e_{ij}^{kl} = e_j^l - e_j^k - e_i^l + e_i^k \quad (47)$$

the law of error propagation gives

$${u_{e_{ij}^{kl}}}^2 = {u_{e_j^l}}^2 + {u_{e_j^k}}^2 + {u_{e_i^l}}^2 + {u_{e_i^k}}^2 - 2u_{e_j^l e_j^k} - 2u_{e_j^l e_i^l} + 2u_{e_j^l e_i^k} + 2u_{e_j^k e_i^l} - 2u_{e_j^k e_i^k} - 2u_{e_i^l e_i^k} \quad (48)$$

and with the expressions in Eqs. (37-46)

$$u_{e_{ij}^{kl}}{}^2 = \left(m_j^{l\,2} + m_j^{k\,2}\right) u_{e_j}{}^2 + \left(m_i^{l\,2} + m_i^{k\,2}\right) u_{e_i}{}^2 - 2m_j^l m_j^k u_{e_j}{}^2 - 2m_j^l m_i^l u_{e_{ji}} + 2m_j^l m_i^k u_{e_{ji}} + 2m_j^k m_i^l u_{e_{ji}} - 2m_j^k m_i^k u_{e_{ji}} - 2m_i^l m_i^k u_{e_i}{}^2 \quad (49)$$

which simplifies to

$$u_{e_{ij}^{kl}}{}^2 = \left(m_j^l - m_j^k\right)^2 u_{e_j}{}^2 + \left(m_i^l - m_i^k\right)^2 u_{e_i}{}^2 \quad (50)$$

For the purpose of uncertainty estimation in baselines of up to a few kilometres (that is, station *i* relatively close to station *j*, therefore very similar apparent receiver-to-satellite elevations) one can also consider $m_j^l = m_i^l$ and $m_j^k = m_i^k$, and write

$$u_{e_{ij}^{kl}}{}^2 = \left(m_j^l - m_j^k\right)^2 \left(u_{e_j}{}^2 + u_{e_i}{}^2\right) \quad (51)$$

This means that the main factor defining the uncertainty in the double-differenced error is the geometry of the particular double difference (given here by the squared difference between m_j^l and m_j^k). For very similar elevations the double-differenced error will be virtually zero whereas in other cases the sum of zenith errors at *i* and *j* will be considerably amplified by the squared difference between mapping functions.

Now let us examine the type of error that cannot be described by a zenith error and a mapping function, that is, the multipath effect and the incorrect modelling of antenna phase center and variations. For these cases, Eqs. (33-46) do not hold and the uncertainties $u_{e_j^l}$, $u_{e_j^k}$, $u_{e_i^l}$ and $u_{e_i^k}$ need to be estimated by the appropriate procedure (see subsections 5.3 and 5.4). The four covariances involving different stations (thus different multipath models or antenna calibrations), $u_{e_j^l e_i^l}$, $u_{e_j^k e_i^k}$, $u_{e_j^l e_i^k}$, and $u_{e_j^k e_i^l}$, can be regarded as zero. For the other two covariances we resort to the definition of the correlation coefficient ρ which permits us to write

$$u_{e_j^l e_j^k} = \rho_{e_j^l e_j^k} u_{e_j^l} u_{e_j^k} \quad (52)$$

$$u_{e_i^l e_i^k} = \rho_{e_i^l e_i^k} u_{e_i^l} u_{e_i^k} \quad (53)$$

These correlation coefficients are unknown. We can either compute them from an available sample or simply assume them to have the value for the worst case, that is, +1 or -1. With this latter assumption, the law of error propagation Eq. (48) results in

$$u_{e_{ij}^{kl}}{}^2 = u_{e_j^l}{}^2 + u_{e_j^k}{}^2 + u_{e_i^l}{}^2 + u_{e_i^k}{}^2 + 2u_{e_j^l} u_{e_j^k} + 2u_{e_i^l} u_{e_i^k} \quad (54)$$

or in more compact form

$$u_{e_{ij}^{kl}}{}^2 = \left(u_{e_j^l} + u_{e_j^k}\right)^2 + \left(u_{e_i^l} + u_{e_i^k}\right)^2 \quad (55)$$

6.2 Propagation from double differences to baseline distance

Having estimated the uncertainty in the double-difference equations - either by Eq. (51) or Eq. (52) depending on whether a mapping function is in use or not for the error - these uncertainties have to be propagated to the distance obtained after the least squares adjustment.

By defining

$$\boldsymbol{M} = \left(\boldsymbol{B^T P B}\right)^{-1}\boldsymbol{B^T P} \tag{56}$$

Eq. (10) can be written as

$$\boldsymbol{x'} = \boldsymbol{M k} \tag{57}$$

The effect of the uncertainties in the double-difference equations used ${u_{e_{ij}^{kl}}}^2$, ${u_{e_{ij}^{km}}}^2$... onto the final distance can be obtained by the law of covariance matrix propagation as

$$\boldsymbol{C_{x'}} = \boldsymbol{M C_k M^T} \tag{58}$$

where

$$\boldsymbol{C_k} = \begin{pmatrix} {u_{e_{ij}^{kl}}}^2 & & \\ & {u_{e_{ij}^{km}}}^2 & \\ & & \ldots \end{pmatrix} \tag{59}$$

So that

$$u_{D_{ij}} = \sqrt{\boldsymbol{C_{x'}}(1,1)} \tag{60}$$

is the estimated uncertainty in the final distance due to the propagated uncertainties of the error source.

In the case of the antenna heights, since their uncertainties are very small quantities we can safely neglect the Earth's curvature for the computation of the propagation of these uncertainties to the final baseline distance D_{ij}. This geometric distance between the baseline endpoints is related to the reduced distance D_{Rij} and the increment of height between stations Δh_{ij}, neglecting the Earth's curvature, by

$$D_{ij} = \sqrt{{D_{Rij}}^2 + {\Delta h_{ij}}^2} \tag{61}$$

The law of error propagation in terms of the uncertainty in one height (say *i*) is

$$u_{D_{ij}} = \frac{\partial D_{ij}}{\partial \Delta h_{ij}} u_{h_i} \tag{62}$$

which gives

$$u_{D_{ij}} = \frac{\Delta h_{ij}}{D_{ij}} u_{h_i} \tag{63}$$

and considering the uncertainties in the antenna heights of both baseline endpoints, *i* and *j*, it is obtained

$$u_{D_{ij}} = \frac{\Delta h_{ij}}{D_{ij}} \sqrt{{u_{h_i}}^2 + {u_{h_j}}^2} \tag{64}$$

Apart from the uncertainty in the measured antenna heights, u_{h_i} and u_{h_j}, the monument instability also affects the final distance. In the case of instability in the vertical component, estimated in pillars *i* and *j* as $u_{h'_i}$ and $u_{h'_j}$, respectively, the uncertainty propagated to the final distance is

$$u_{D_{ij}} = \frac{\Delta h_{ij}}{D_{ij}} \sqrt{{u_{h'_i}}^2 + {u_{h'_j}}^2} \tag{65}$$

The horizontal component of the monument instability transfers directly to the horizontal (reduced) distance. Assuming it is estimated in pillars *i* and *j* as u_{DR_i} and u_{DR_j}, respectively, it propagates to the final (slant) distance in a way that can be computed similarly to the derivation in Eqs. (61)-(64). That is, for a horizontal error u_{DR_i} in pillar *i*

$$u_{D_{ij}} = \frac{\partial D_{ij}}{\partial D_{Rij}} u_{D_{Ri}} \tag{66}$$

which, by means of Eq. (61), gives

$$u_{D_{ij}} = \frac{D_{Rij}}{D_{ij}} u_{h_i} \tag{67}$$

and considering the horizontal instabilities in both pillars, u_{DR_i} and u_{DR_j}, respectively, it is obtained

$$u_{D_{ij}} = \frac{D_{Rij}}{D_{ij}} \sqrt{{u_{DR_i}}^2 + {u_{DR_j}}^2} \tag{68}$$

As an alternative to the use of Eqs. (65) and (68) for propagation to the final distance of the vertical and horizontal monument instabilities, respectively, it is safer to add up in

quadrature all four components as representing the worst case of the monument configuration

$$u_{D_{ij}} = \sqrt{{u_{h\prime_i}}^2 + {u_{DR_i}}^2 + {u_{h\prime_j}}^2 + {u_{DR_j}}^2} \tag{69}$$

6.3 Uncertainty budget

The uncertainty budget in the baseline distance D_{ij} propagated from the error sources, $U_{D_{ij}}$ (with k = 2) results as

$$U_{D_{ij}} = \sqrt{{U_{D_{ij\_tr}}}^2 + {U_{D_{ij\_ion}}}^2 + {U_{D_{ij\_mp}}}^2 + {U_{D_{ij\_ant\_cal}}}^2 + {U_{D_{ij\_ant\_h}}}^2 + {U_{D_{ij\_instab}}}^2} \tag{70}$$

where $U_{D_{ij\_tr}}$, $U_{D_{ij\_ion}}$, $U_{D_{ij\_mp}}$, $U_{D_{ij\_ant\_cal}}$, $U_{D_{ij\_ant\_h}}$ and $U_{D_{ij\_instab}}$ are the uncertainties of the double differenced tropospheric delay, ionospheric delay, multipath effect, antenna calibration, antenna height and monument instability, respectively, that is, those designated by $u_{D_{ij}}$ in the previous sections now scaled with a factor k = 2.

Tables in Section 7 Application Example provide numerical values for these uncertainties.

7 APPLICATION EXAMPLE

We use a baseline from the CERN geodetic network, which was observed by GNSS techniques between July 11 and July 14, 2022, by members of the Universitat Politècnica de València (UPV) and the Institut National de l'information Géographique et forestière (IGN) as part of the CERN network observation campaign carried out for the Geometre project [1]. GNSS receivers were used along with individually calibrated choke ring antennas to observe with an observing rate of 1 s and no elevation mask the satellites of the four global constellations (GPS, Galileo, GLONASS and BeiDou). In this example we use the longest (approximately 6.5 km) of the five baselines observed, namely the baseline from pillar named P233 to pillar named P231, and the RINEX observation files decimated to a sampling rate of 30 s that are given in [30] along with the ANTEX antenna calibration files, so that the study can be reproduced by the interested reader.

As mentioned in Section 3, we start with the initial information obtained from the CSRS-PPP service [16] after uploading the observation files: approximate coordinates, receiver clocks, tropospheric delays, and carrier phase residuals.

7.1 Example uncertainty budget

As an example, the first common epoch (July 11, 2022, 16:11:30 GPS time) for satellites G01 and G31 is taken. The L3 double-differenced observation ($\lambda\varphi_{ij}^{kl}$) needs to be corrected for the tropospheric delay (T_{ij}^{kl}), the multipath effect (MP_{ij}^{kl}) and the antenna

calibration (AC_{ij}^{kl})

$$\lambda\varphi_{ij}^{kl}{}_{c} = \lambda\varphi_{ij}^{kl} - T_{ij}^{kl} - MP_{ij}^{kl} - AC_{ij}^{kl} \quad (71)$$

The corresponding uncertainty budget is shown in Table 7.1. The standard uncertainty of the observed double-differenced phase can be estimated from a previous zero-baseline essay (such as 0.7 mm [3, pp.4-5] amplified by the 3.0 factor due to the formation of L3 combination [15, p.53]). In any case, it has little importance for the total uncertainty contribution since the other errors predominate. For the case of the tropospheric delay, the values from CSRS-PPP at the zero-difference level are used. The sidereal filtering technique is used to obtain the values for multipath. For the antenna calibration, individual calibrations are used (performed with the anechoic chamber method by the IGG, Universität Bonn) and their comparison with latest IGS ANTEX generic antenna calibration model available at the time of the observation for the computation of standard uncertainties.

Table 7.1. Uncertainty budget for the example double-differences phase observation

Quantity	Estimate	Estimated uncertainty ($2u$)	Probability distribution	Standard uncertainty ($1u$)	Sensitivity coefficient	Uncertainty contribution
$\lambda\varphi_{ij}^{kl}$	7983.8416 m	0.0042 m	Normal	0.0021 m	1.0	0.0021 m
T_{ij}^{kl}	0.1190 m	0.0015 m	Normal	0.0008 m	1.0	0.0008 m
MP_{ij}^{kl}	0.0002 m	0.0239 m	Normal	0.0119 m	1.0	0.0119 m
AC_{ij}^{kl}	-0.0004 m	0.0279 m	Normal	0.0140 m	1.0	0.0140 m
$\lambda\varphi_{ij}^{kl}{}_{c}$	7983.7228 m					0.0185 m
					$k = 2$	0.0370 m

As said, this is only an example of an observation that generates one equation of the system of equations. This system has thousands of observations of this type with very different correction values and very different uncertainties: this will be studied in more depth in the following subsection. The solution to obtain the distance after the least squares adjustment has to include the rigorous propagation of the uncertainty for each observing equation as explained in Section 6.

To complete the example, the results for the distance computed with the first 8 h of observations are given in Table 7.2. Apart from the previous error sources, the antenna height determination and the pillar instability are now considered.

With the use of a high-grade surveying TS, we assume an accuracy of 0.1 mm in the determination of the antenna height in each pillar, $u_{hi} = u_{hj} = 0.1$ mm, which, by means of Eq. (64) represents an uncertainty in the distance u_{Dij} below the hundredth of a mm for the current height difference of 212 m and the baseline distance of 6542 m, and therefore it is a value completely negligible. This is also the case of the horizontal instrument centering, whose possible inaccuracy can be neglected.

For the monument stability during the three-day observation period, we estimate in 0.1 mm the possible maximum height variation in each pillar and, considering a temperature variation of 22 K, and a pillar height and diameter of 1.2 m and 0.4 m, respectively, a maximum horizontal variation of 0.49 mm according to the previous formula (30). By using Eq. (69) this yields an uncertainty in the distance u_{Dij} of 0.71 mm (k = 2).

Table 7.2. Uncertainty budget for the distance computed with the data from 11 July 2022 16:11:30 to 12 July 2022,00:11:30 (GPS time)

Quantity	Estimate	Estimated uncertainty ($2u$)	Probability distribution	Standard uncertainty ($1u$)	Sensitivity coefficient	Uncertainty contribution
D_{ij}	6542.0125 m	0.0008 m	Normal	0.0004 m	1.0	0.0004 m
$\delta_{ant.h_{ij}}$	0.0000 m	0.0000 m	Normal	0.0000 m	1.0	0.0000 m
$\delta_{pillar\ inst_{ij}}$	0.0000 m	0.0007 m	Normal	0.0004 m	1.0	0.0004 m
$D_{ij\ c}^{kl}$	6542.0125 m					0.0006 m
					k = 2	0.0011 m

7.2 Additional insights on uncertainty propagation

A value for the distance can be obtained by Eq. (10) using the observations of the entire time span. It is also possible, and more informative, to group the observations in computation blocks of fixed length (say 8 h) and analyze the values obtained in the different solutions. A central value and corresponding dispersion measure can be obtained for the average in each time block, Fig. 7.1. In the current example, we can see a good agreement between the different solutions. The weighted average value gives a final value for the distance of 6542.0130 m.

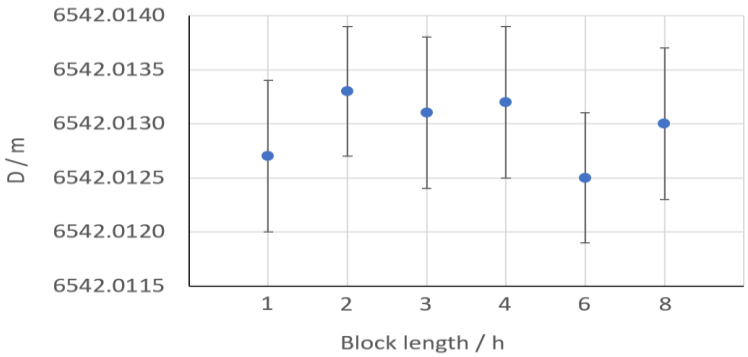

Figure 7.1. Baseline distance P233-P231, values in m. The average values for each of the different time blocks are indicated with the blue dots and the dispersion of the average (k = 2) with the error bars.

For the case of the tropospheric delay, whose uncertainty can be obtained from CSRS-PPP files at the zero-difference level, the propagation to double differences equations by Eq. (51) results in the uncertainties shown in Fig. 7.2 for the first block of eight observation hours.

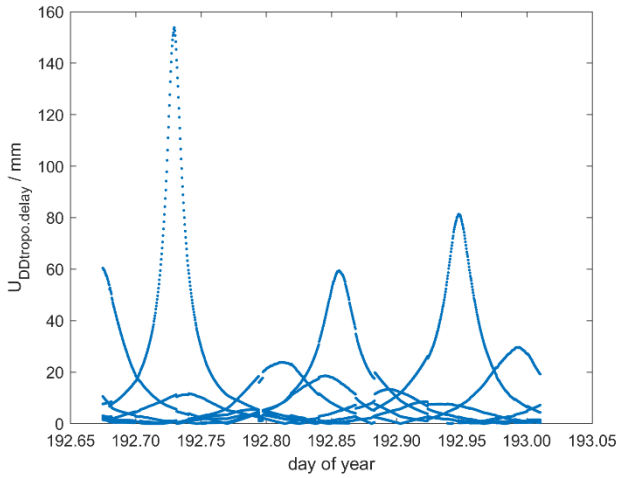

Figure 7.2. Uncertainty in the double differenced tropospheric delay correction (11 July 2022 16:11:30 to 12 July 2022 0:11:30 GPS time).

The different lines refer to the differ satellite pairs used for the corresponding double difference equation. The significant baseline height difference, 211.6 m approximately, already suggested before the computation that the tropospheric delay would not be cancelled after double differencing. Here it can be seen that it may be as large as 15 cm for a particular double difference.

The propagation of these uncertainties in the double-difference equations along the system of equations solution resulting in the final distance determination, Eqs. (58) - (60), yields 0.0006 m for this observation time span. In general, the longer the time span the lower the uncertainty in the distance, as expected, until a value of around 6-8 hours is reached where the decrease in uncertainty is insignificant. This can be seen in Fig. 7.3, where the resulting uncertainties in the distance in terms of the observation time spans are given.

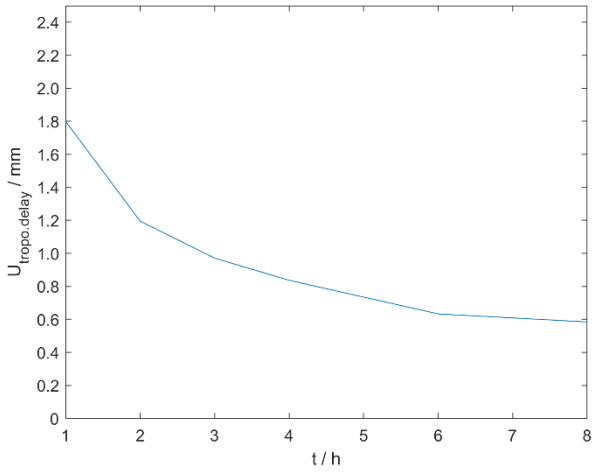

Figure 7.3. Uncertainty in the baseline distance propagated from the tropospheric delay uncertainty for different observation time spans in hours (average values for all the different time blocks).

It is emphasized that these results on the propagation of the uncertainty in tropospheric delay correction up to the final distance depend on the baseline studied, that is, its location, orientation, slope and distance, as well as on the moment of observation (observation start, time span, available observables, etc.) That is, the conclusions drawn are particular to this experiment and cannot be extrapolated to other experiments.

As for the ionospheric delay, in the present case the differences between the calculation with L3 and L1 corrected with the Klobuchar model are negligible. As explained above, the corresponding uncertainty is taken as zero. Alternatively, in the future, if CSRS-PPP values for the ionospheric delay together with their uncertainties become available, these can be corrected from the L1 observation and the uncertainty of the correction be propagated to the final result as in the tropospheric delay case above. Although of negligible magnitude, as expected, this result can be of formal interest in the elaboration of the full uncertainty budget for L1.

Regarding the multipath effect, after constructing multipath correction models for the different satellites as explained in section 5.3, e.g. Fig. 7.4 for satellite G03 and station P231, we can obtain the corresponding uncertainties in double differences by using Eq. (55), Fig. 7.5.

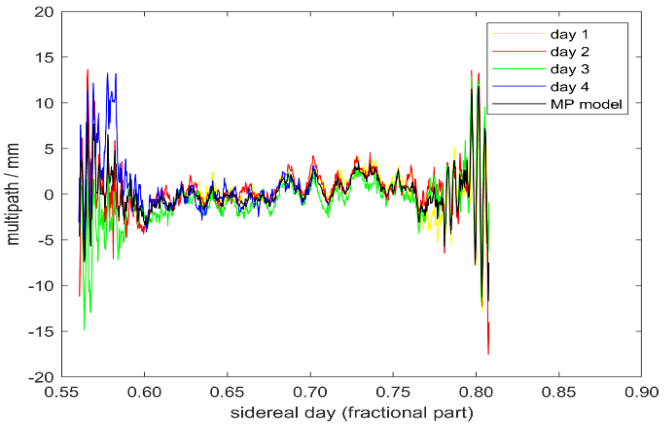

Figure 7.4. Multipath correction model for satellite G03 (station P231)

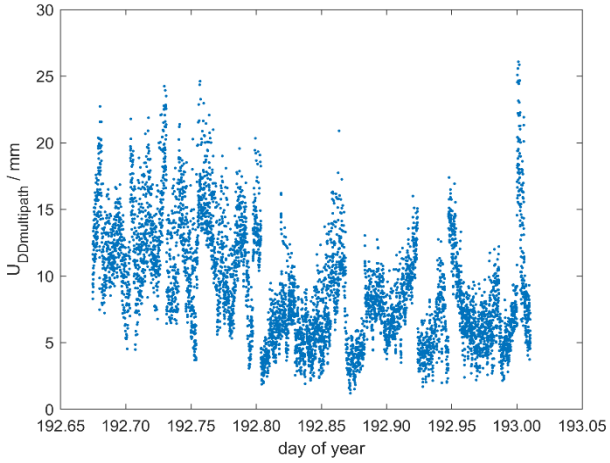

Figure 7.5. Uncertainty in the double differenced multipath correction (11 July 2022 16:11:30 to 12 July 2022 0:11:30 GPS time)

The propagation to the final distance, Eqs. (58) - (60), gives 0.0003 m for the observation time span in Fig. 7.5. In this case, as it can be seen, the contribution to the uncertainty in the final distance, Fig. 7.6, is smaller than it was for the tropospheric delay, Fig. 7.3.

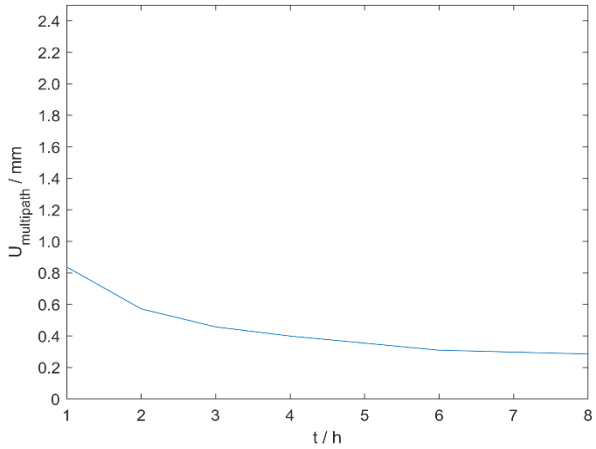

Figure 7.6. Uncertainty in the baseline distance propagated from the multipath uncertainty for different observation time spans in hours (average values for all the different time blocks)

Regarding the antenna calibration uncertainties, we present here the results after estimating the uncertainty by means of the comparison between the available individual antenna calibrations (performed with the anechoic chamber method by the IGG, Universität Bonn) and the latest IGS ANTEX generic antenna calibration model available at the time of the observation. At the zero-difference level there are discrepancies of up to a few mm between the individual and generic calibration, which by using Eq. (55), may lead to uncertainties in the double difference values up to a couple of cm, as it is shown in Fig. 7.7.

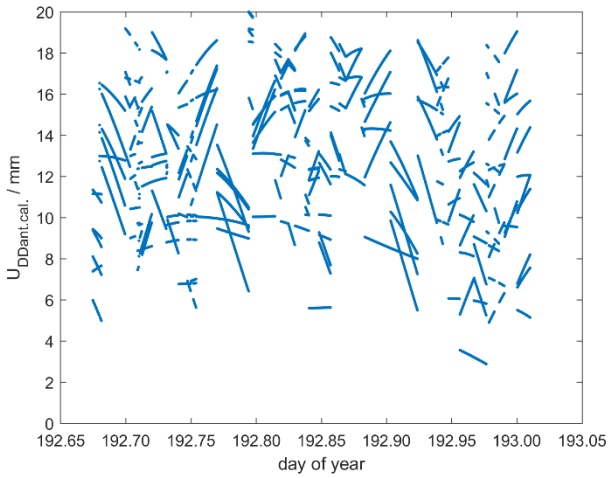

Figure 7.7. Uncertainty in the double differenced antenna calibration (11 July 2022 16:11:30 to 12 July 2022 0:11:30 GPS time).

The propagation to the final distance, computed by Eqs. (58)-(60), gives 0.0004 m for this observation time span. As expected, the longer the time span the lower the uncertainty for the distance up to a time span of around 6-8 hours where the decrease is minimal, Fig. 7.8.

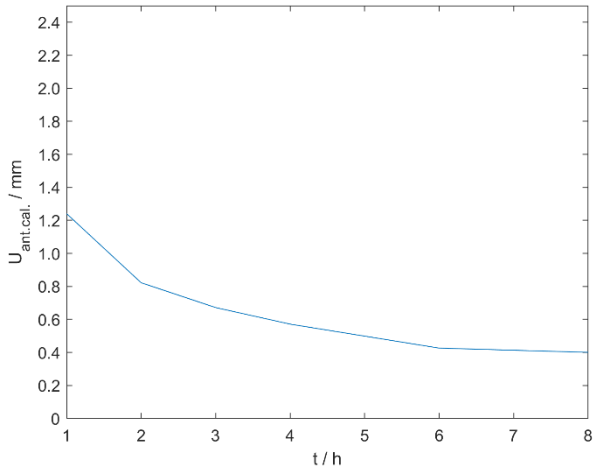

Figure 7.8. Uncertainty in the baseline distance propagated from the antenna calibration uncertainty for different observation time spans in hours (average values for all the different time blocks).

The total uncertainty budget for k = 2 (95% level of confidence) is given in Table 7.3. As it can be seen, a large part of the uncertainty is in the troposphere delay due to the height difference of the current baseline, but obviously this could be different for other cases of application. Fig. 7.9 shows the final uncertainty in terms of the observation time span.

Table 7.3. Total uncertainty budget in the baseline distance propagated from all error sources, k = 2, values in mm (average values for all the different time blocks).

Obs. time span / h	$U_{\text{tropo.delay}}$ / mm	$U_{\text{multipath}}$ / mm	$U_{\text{ant.cal.}}$ / mm	$U_{\text{ant.h.}}$ / mm	U_{instab} / mm	U_{total} / mm
1	1.80	0.84	1.24	0.00	0.71	2.45
2	1.20	0.57	0.82	0.00	0.71	1.72
3	0.97	0.46	0.67	0.00	0.71	1.45
4	0.83	0.40	0.57	0.00	0.71	1.30
6	0.63	0.31	0.43	0.00	0.71	1.09
8	0.58	0.29	0.40	0.00	0.71	1.04

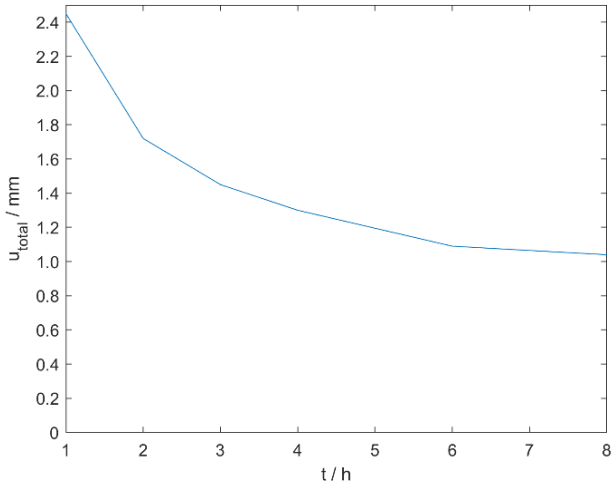

Figure 7.9. Total uncertainty in the baseline distance propagated from all error sources for different observation time spans in hours (average values for all the different time blocks).

8 REFERENCES

[1] Pollinger F, Baselga S, Courde C, Eschelbach C, García-Asenjo L, Garrigues P, Guillory J, Hedekvist PO, Helojärvi T, Kallio, U, Klügel T, Köchert P, Lösler M, Luján R, Meyer T, Neyezhmakov P, Pesce D, Pisani M, Poutanen M, Prellinger G, Röse A, Seppä J, Truong D, Underwood R, Wezka K, Wallerand JP and Wiśniewski M 2022, The European GeoMetre project – developing enhanced large-scale dimensional metrology for geodesy. Proc. 5th Joint International Symposium on Deformation Monitoring (JISDM), June 20-22, Valencia, Spain.

[2] Bauch A, Eusébio L, Kallio U, Koivula H, Lahtinen S, Marques F, Pellegrino O, Pires C, Pollinger F, Poutanen M, Saraiva F, Schön S and Zimmermann F 2017, Good practice guide for high accuracy global navigation satellite system based distance metrology. Revised Version 2. (Braunschweig: JRP SIB60 Surveying Consortium).

[3] García-Asenjo L, Baselga S, Atkins C and Garrigues P 2021, "*Development of a Submillimetric GNSS-Based Distance Meter for Length Metrology*", Sensors 21 1145 21 pp.

[4] Baselga S, García-Asenjo L, Garrigues P, and Luján R 2022, "*GBDM+: An improved methodology for a GNSS-Based Distance Meter*", Meas. Sci. Technol. 33 085020 (16pp).

[5] Altamimi, Z., Rebischung, P., Collilieux, X. et al. 2023, "*ITRF2020: an augmented reference frame refining the modeling of nonlinear station motions.*" J Geod 97, 47. https://doi.org/10.1007/s00190-023-01738-w

[6] Gervaise J 1983, First results of the geodetic measurements carried out with the Terrameter, two wavelength electronic distance measurement instrument. Geodätischen Seminar über Elektrooptische Präzisionsstreckenmessung, September 23, Munich, Germany, 213-229.

[7] Jokela J and Häkli P 2006, Current Research and Development at the Nummela Standard Baseline, Proc. Shaping the Change, XXIII FIG Congress, October 8-13, Munich, Germany, 15 pp.

[8] Curtis CJ 1992, Calibration and use of the Mekometer ME5000 in the survey of the Channel Tunnel, Proc. Use and calibration of the Kern ME 5000 mekometer, June 18-19, Stanford, United States, 67-82.

[9] USGS Eathquake Hazards Program, Two-color Electronic Distance Meter (EDM), https://earthquake.usgs.gov/monitoring/deformation/edm, electronic resource, last accessed March 31, 2022.

[10] Bureau International des Poids et Mesures (BIPM) 2022, The International System of Units (SI). 9th edition 2019, v2.01 December 2022. https://www.bipm.org/documents/20126/41483022/SI-Brochure-9-EN.pdf, accessed 24 October 2023.

[11] Defraigne, P. et al 2022, "*Achieving traceability to UTC through GNSS measurements*". Metrologia 59 064001.

[12] Collilieux X, Métivier L, Altamimi Z, van Dam T and Ray J 2011, "*Quality assessment of GPS reprocessed terrestrial reference frame*", GPS Solut. 15(3) 219-231.

[13] Wezka K, García-Asenjo L, Próchniewicz D, Baselga S, Szpunar R, Garrigues P, Walo J, Luján R 2022, EDM-GNSS distance comparison at the EURO5000 calibration baseline: preliminary results. 5th Joint International Symposium on Deformation Monitoring (JISDM), June 20-22, Valencia, Spain.

[14] Xu G, Shen Y, Yang Y, Sun H, Zhang Q, Guo J and Yeh TK 2010, Equivalence of GPS Algorithms and Its Inference, in Xu G (Ed.), Sciences of Geodesy – I, Springer-Verlag Berlin Heidelberg, 219-273.

[15] Dach R, Lutz S, Walser P, Fridez P (Eds) 2015, Bernese GNSS Software Version 5.2. User manual (Astronomical Institute, University of Bern: Bern Open Publishing).

[16] Banville S, Hassen E, Lamothe P, Farinaccio J, Donahue B, Mireault Y, Goudarzi MA, Collins P, Ghoddousi-Fard R, Kamali O 2021, "*Enabling ambiguity resolution in CSRS-PPP*", Navigation 68(2) 433-451.

[17] Atiz OM and Kalayci I 2021, "*Performance Assessment of PPP-AR positioning and zenith total delay estimation with modernized CSRS-PPP*", Artificial Satellites 56(2) 18-34.

[18] Mendez-Astudillo J, Lau L, Tang Y-T and Moore T 2018, "*Analysing the zenith tropospheric delay estimates in on-line Precise Point Positioning (PPP) services and PPP software packages*", Sensors 18 580 (16 pp).

[19] Leick A, Rapoport L and Tatarnikov D 2015, GPS Satellite Surveying 4th Ed. (Hoboken, New Jersey: John Wiley and Sons, Inc.).

[20] Teunissen PJG and Montenbruck O (Eds.) 2017, Springer Handbook of Global Navigation Satellite Systems (Cham, Switzerland: Springer).

[21] Baselga S 2014, "*Ambiguity-Free Method for Fast and Precise GNSS Differential Positioning*", Journal of Surveying Engineering 140(1) 22–27.

[22] Black HD and Eisner A 1984, "*Correcting satellite Doppler data for tropospheric effects*", Journal of Geophysical Research 89 2616-2626.

[23] Niell AE 1996, "*Global mapping functions for the atmosphere delay at radio wavelengths*", Journal of Geophysical Research 101 3227-3246.

[24] Boehm J, Werl B and Schuh H 2006, "*Troposphere mapping functions for GPS and very long baseline interferometry from European Centre for Medium-Range Weather Forecasts operational analysis data*", Journal of Geophysical Research 111 B02406.

[25] Boehm J, Niell A, Tregoning P and Schuh H 2006, "*Global Mapping Function (GMF): A new empirical mapping function based on numerical weather model data*", Geophysical Research Letters 33 L07304.

[26] Kallio U, Koivula H, Lahtinen S, Nikkonen V and Poutanen M 2019, "*Validating and comparing GNSS antenna calibrations*", Journal of Geodesy 93 1–18.

[27] Bergstrand S, Jarlemark P and Herbertsson M 2020, "*Quantifying errors in GNSS antenna calibrations: Towards in situ phase center corrections*", Journal of Geodesy 94 105 (15 pp).

[28] Haas R, Bergstrand S and Lehner W 2013, "*Evaluation of GNSS Monument Stability*". In: Altamimi, Z., Collilieux, X. (eds) Reference Frames for Applications in Geosciences. International Association of Geodesy Symposia, vol 138. Springer, Berlin, Heidelberg. https://doi.org/10.1007/978-3-642-32998-2_8.

[29] Močnik R, Koler B, Zupan D, Ambrožič T 2019, "*Investigation of the Precision in Geodetic Reference-Point Positioning Because of Temperature-Induced Pillar Deflections*", Sensors 2019, 19, 3489 (13 pp).

[30] García-Asenjo L, Baselga S, Garrigues P, Lujan R and Pesce D 2025, Dataset for the Good practice guide on high-accuracy GNSS-based distance metrology. https://doi.org/10.5281/zenodo.15019017, accessed 13 March 2025.

EURAMET e.V.
Bundesallee 100
38116 Braunschweig
Germany

Phone: +49 531 592 1960
Fax: +49 531 592 1969
E-mail: secretariat@euramet.org

The EMPIR initiative is co-funded by the European Union's Horizon 2020 research and innovation programme and the EMPIR Participating States